Journal of Colloid and Interface Science 594 (2021) 759–769

Contents lists available at ScienceDirect

Journal of Colloid and Interface Science

journal homepage: www.elsevier.com/locate/jcis

Regular Article

Surface modification of silica nanoparticles by hexarhenium anionic cluster complexes for pH-sensing and staining of cell nuclei

Alsu Khazieva [a,*], Kirill Kholin [a], Irek Nizameev [a], Konstantin Brylev [b], Ilya Kashnik [b], Alexandra Voloshina [a], Anna Lyubina [a], Aidar Gubaidullin [a], Amina Daminova [c], Konstantin Petrov [a], Asiya Mustafina [a,*]

[a] Arbuzov Institute of Organic and Physical Chemistry, FRC Kazan Scientific Center of RAS, 8 Arbuzov str., 420088 Kazan, Russian Federation
[b] Nikolaev Institute of Inorganic Chemistry SB RAS, 3 Acad. Lavrentiev Ave., 630090 Novosibirsk, Russian Federation
[c] Kazan (Volga region) Federal University, 18 Kremlyovskaya str., 420008 Kazan, Russian Federation

GRAPHICAL ABSTRACT

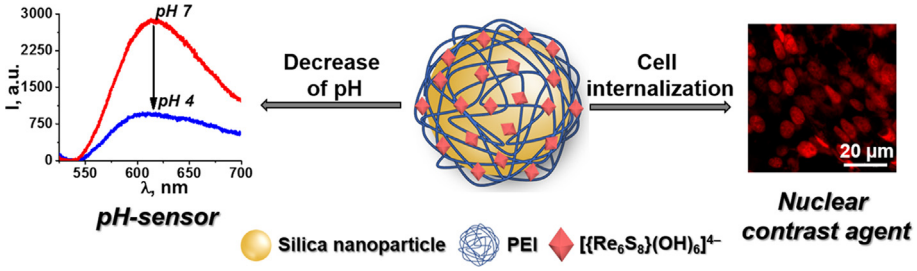

ARTICLE INFO

Article history:
Received 28 December 2020
Revised 5 March 2021
Accepted 13 March 2021
Available online 19 March 2021

Keywords:
Silica nanoparticles
Hexarhenium cluster
Luminescence
Cellular contrast agent
pH-sensing
Polyethyleneimine
Cell internalization

ABSTRACT

The surface deposition of luminescent anionic cluster complex $[\{Re_6S_8\}(OH)_6]^{4-}$ advantages to the design and synthesis of composite luminescent silica nanoparticles (SNs) for intracellular imaging and sensing, while the encapsulation of the cluster units into SNs lacks for efficient luminescence. The deposition of the Re_6 clusters resulted from their assembly at the silica surface functionalized by amino-groups provides the synthetic route for the composite SNs with bright cluster-centered luminescence invariable in pH range from 4.0 to 12.0. The pH-dependent supramolecular assembly of the cluster units with polyethyleneimine (PEI) at the silica surface is an alternative route for the synthesis of the composite SNs with high cluster-centered luminescence sensitive to pH-changes within 4.0–6.0. The sensitivity derives from the pH-driven conformational changes of PEI chains resulting in the release of the clusters from the PEI-based confinement under the acidification within pH 6.0–4.0. The potential of the composite SNs in cellular contrasting has been also revealed by the cell viability and flow cytometry measurements. It has been found that the PEI-supported embedding of the cluster units facilitates cell internalization of the composite SNs as well as results in specific intracellular distribution manifested by efficient staining of the cell nuclei in the confocal images.

1. Introduction

Both transparency of silica matrix and endocytosis-driven cell internalization make silica nanoparticles (SNs) promising basis for design of sensors, carriers for therapeutic and luminescent cellular contrasting agents [1–7]. The aforesaid functional properties can be achieved by incorporation of building blocks with different functionality into SNs with a formation of hybrid SNs. Literature data represent diverse synthetic routes for synthesis of hybrid SNs [8–15], although highlighting of optimal synthetic routes for combination of sensing and cellular contrasting functions in each

* Corresponding authors.
E-mail address: alsu_mukhamet@mail.ru (A. Khazieva).

https://doi.org/10.1016/j.jcis.2021.03.082
0021-9797/

hybrid SN is still challenging problem. The present work is focused on optimization of hybrid SNs for joining of efficient red emission and sensing function with efficient cell internalization. Thus, comparative analysis of different synthetic routes for incorporation of polyionic functional building blocks exemplified by metal complexes and polyelectrolytes into SNs is introduced herein in correlation with the functional properties of the hybrid SNs.

Polyelectrolytes bearing pH-dependent groups are a top of current interest, since their pH-triggered rearrangement of is widely applied in the design of carriers with a drug delivery function [16,17], where the acidification arisen from the early-to-late endosome conversion can trigger the drug delivery [18]. The visualization of the pH-triggered rearrangements of polyelectrolytes at a silica/water interface through the use of luminescent probes can help in deeper recognition of the effect of early-to-late endosome transformation on cytotoxicity of the silica nanomaterial. Thus, the present work is aimed at visualization of pH-triggered rearrangements of polyelectrolytes at a silica/water interface by means of ionic red-emitting cluster complexes as the luminescent probes.

Octahedral metal cluster complexes based on $\{M_6(\mu_3\text{-}X)_8\}^{4+}$ (M = Mo or W; X = Cl, Br or I) and $\{Re_6(\mu_3\text{-}Q)_8\}^{2+}$ (Q = S or Se) cores have been gaining growing attention as building blocks of nanomaterials for biomedical applications [19–33]. The latter derives from the unique photoluminescence and high stability of $\{M_6(\mu_3\text{-}X)_8\}^{4+}$ and $\{Re_6(\mu_3\text{-}Q)_8\}^{2+}$ cluster cores, where X or Q is a face-capping ligand. Each metal atom of the cluster core is additionally coordinated by an inorganic or organic apical ligand L leading to a $[\{M_6Y_8\}L_6]^n$ ionic or molecular complex. The aforesaid is the reason for the choice of hexanuclear clusters as the ionic building blocks in the design of a stimuli-responsive luminescent nanomaterial. The focusing on $[\{Re_6S_8\}(OH)_6]^{4-}$ complex is due to its suitability for sensing arisen from very quick aquation of apical positions realized through a protonation of the apical hydroxo ligands, which was for the first time reported by Brylev et al. [34], and later was successfully used for monitoring the acidification derived from the enzymatic hydrolysis of acetylcholine [35]. However, the easy aquation of $[\{Re_6S_8\}(OH)_6]^{4-}$ restricts the applicability of the pH-sensitive cluster-centered luminescence in intracellular imaging and sensing, since it results in the precipitation of the neutral aquahydroxo complex $[\{Re_6S_8\}(H_2O)_4(OH)_2]$ in aqueous solutions [34,36]. Nevertheless, the stability of $[\{Re_6S_8\}(OH)_6]^{4-}$ can be significantly increased under either encapsulation of the cluster into dendritic nanostructure decorated by dialkyl-amino/ammonium groups [37] or the wrapping by polyethyleneimine (PEI) chains [36].

This highlights an impact of the electrostatic attraction between amino/ammonium groups and the cluster units as the route of their incorporation into SNs, which was successfully applied for deposition of the hexamolybdenum clusters on the silica surface decorated by amino-groups [14,15]. Moreover, the well-known ability of PEI chains to wrap around naked silica nanoparticles resulting in their recharging from negative to positive [13] also provides a basis for a deposition of the negatively charged cluster units. The above-stated introduces both covalent surface modification by amino-groups and adsorption of PEI on the naked silica surface as the routes for deposition of $[\{Re_6S_8\}(OH)_6]^{4-}$ on the surface of SNs. However, the encapsulation of the cluster into SNs will be also applied, since the successful inclusion of $[\{Re_6S_8\}(OH)_6]^{4-}$ into silica spheres was previously reported [19]. Thus, the following synthetic modes will be used for the cluster incorporation into SNs: (1) $[\{Re_6S_8\}(OH)_6]^{4-}$ will be directly bound with amino/ammonium groups embedded to the silica surface; (2) the embedding of $[\{Re_6S_8\}(OH)_6]^{4-}$ with the "naked" non-modified silica surface will be facilitated by PEI; (3) encapsulation or the so-called "doping" of the cluster into silica spheres. The luminescence of the cluster units embedded onto the SNs and its pH-sensitivity will be correlated with the size, charge and structure of the exterior layer of the SNs. The cellular imaging ability of the SNs will be also introduced in order to choose the optimal nanoparticles in staining of cell nuclei.

2. Experimental Section

2.1. Materials

Tetraethyl orthosilicate (TEOS, 98%), ammonium hydroxide (28–30%), *n*-heptanol (98%), 3-aminopropyltriethoxysilane (APTES, 99%), 4-morpholineethanesulfonic acid hydrate (MES, 99%), *β*-alanine (99%) and fluorescamine (pure) were purchased from Acros Organics and used without further purification. Triton X-100 (laboratory grade), cyclohexane (99%), polyethyleneimine (PEI, Quality Level – 200), KCl (≥99%), NaOH (≥98%) and $NaHCO_3$ (≥99.7) were purchased from Sigma-Aldrich. *Tris*-(hydroxymethyl)-aminomethane (TRIS, 98%) was purchased from Scharlau.

The salt $K_4[\{Re_6S_8\}(OH)_6]\cdot 8H_2O$ was synthesized and purified in accordance with the previously published procedures [38].

TEOS was purified by distillation.

2.2. Synthesis

Synthesis of silica nanoparticles (SNs) was performed through the water-in-oil microemulsion procedure. The mixture of Triton X-100 (4.76 g), *n*-heptanol (4.58 mL), cyclohexane (18.64 mL), TEOS (0.4 mL), and a 2.2 mL of water was prepared and stirred for 30 min. Then, additionally prepared solution containing Triton X-100 (4.76 g), *n*-heptanol (4.58 mL), cyclohexane (18.64 mL), and aqueous solutions of NH_3 (28–30%) was added to the mixture, followed by stirring for 24 h.

Synthesis of amino-modified silica nanoparticles ($SNsNH_2$) was performed through the water-in-oil microemulsion procedure. The synthetic mixture from Triton X-100 (8.63 g), cyclohexane (33.75 mL), *n*-heptanol (8.1 mL) and 2.16 mL of water was stirred for 15 min, followed by the addition of 0.27 mL of aqueous ammonia (28–30%). After stirring for 15 min, TEOS (0.23 mL) was added to the mixture, followed by further stirring for 24 h. Then, TEOS (0.23 mL) was added again, and the mixture was stirred for 30 min. After addition of APTES (0.045 mL), the mixture was stirred for another 24 h.

Synthesis of amino-modified cluster-doped silica nanoparticles ($[Re_6]@SNsNH_2$) was performed through the water-in-oil microemulsion procedure. The synthetic mixture from Triton X-100 (4.32 g), cyclohexane (16.88 mL), *n*-heptanol (4.05 mL) and 1.08 mL of the aqueous solution of $K_4[\{Re_6S_8\}(OH)_6]\cdot 8H_2O$ (C = 2.5 mM) was stirred for 15 min, followed by the addition of 0.135 mL of aqueous ammonia (28–30%). After stirring for 15 min, TEOS (0.115 mL) was added to the mixture, followed by further stirring for 24 h. Then, TEOS (0.115 mL) was added again, and the mixture was stirred for 30 min. After addition of APTES (0.0225 mL), the mixture was stirred for another 24 h.

The synthesized nanoparticles were separated from the microemulsion by adding acetone, centrifuging, and washing with acetone/ethanol mixture (1:1), ethanol (once) and water (several times).

Fluorescamine-based procedure was applied for quantitative assay of amino groups on the surface of the aminomodified SNs [39].

The ionic assembly of the PEI-SNs with $[\{Re_6S_8\}(OH)_6]^{4-}$ has been performed according to the following procedure. The aqueous colloids of the SNs (0.5 $g\cdot L^{-1}$) were mixed with excess aqueous solution polyethyleneimine (PEI) (18 $g\cdot L^{-1}$, pH = 7.0, adjusted by HCl). The mixture was sonicated for 15 min with further phase

separation by centrifugation at 4 °C (15000 rpm, 15 min) in order to get rid of excess PEI. The obtained silica nanoparticles, decorated by PEI (PEI-SNs), were mixed with aqueous solution of cluster complex (0.035 mM). The mixture was sonicated for 15 min with further phase separation by centrifugation at 4 °C (15000 rpm, 15 min) in order to get rid of excess cluster units. Afterwards, the assembled nanoparticles ($[Re_6]$-PEI-SNs) were washed and dispersed in water.

The ionic assembly of the $SNsNH_2$ with $[\{Re_6S_8\}(OH)_6]^{4-}$ cluster anions has been performed by mixing of the aqueous solution of cluster complex (0.035 mM) with the aqueous colloids of the $SNsNH_2$ (0.5 $g{\cdot}L^{-1}$). The mixture was stirred by means of Shaker Hei-MIX Multi Reax for 30 min and left for 4 days in a dark place. Afterwards, obtained assembled nanoparticles ($[Re_6]$-$SNsNH_2$) were separated by centrifugation at 4 °C (15000 rpm, 15 min) in order to get rid of excess cluster units. Thereafter, $[Re_6]$-$SNsNH_2$ were washed and dispersed in water.

The *$[Re_6]$-PEI* was obtained by mixing aqueous solutions of the $[\{Re_6S_8\}(OH)_6]^{4-}$ cluster complex and PEI (pH = 7.0, adjusted by HCl) at molar ratio 1:1.

2.3. Methods

Detailed descriptions of dynamic light scattering (DLS) and pH measurements, electronic absorption, steady state and time resolved luminescence, inductively coupled plasma optical emission spectrometry (ICP-OES), small angle X-Ray scattering (SAXS) [40,41], powder X-ray diffraction (PXRD) [42], transmission electron microscopy (TEM) imaging, cytotoxicity and flow cytometry assays are presented in Supplementary materials. The represented values are average of three repeated measurements.

The pH values in the aqueous dispersions were adjusted by the use of the buffer systems, which are acetic-acetate (pH = 4.0 and 5.0), MES (pH = 5.4 and 6.0), TRIS (pH = 7.0, 8.0, and 9.0), carbonate (pH = 10.0 and 10.9) and KCl–NaOH (pH = 12.0).

The cell culture of M−Hela from the collection of the Institute of Cytology of the Russian Academy of Sciences and human Chang Liver cell line from N. F. Gamaleya Research Center of Epidemiology and Microbiology were used in the experiments. The standard nutrient medium "Igla" with an addition of 10% calf serum and 1% essential amino acids was purchased from the Chumakov Institute of Poliomyelitis and Viral Encephalitis (Moscow, Russia).

The cell samples (M−HeLa and Chang Liver) were analyzed after 24-hour incubation by the SNs.

3. Results and discussion

3.1. Synthesis and characterization of the composite SNs

As it has been already demonstrated amino/ammonium groups at a silica surface can facilitate a deposition of anionic complexes [13,14]. The synthesis of amino-modified silica nanoparticles ($SNsNH_2$) was performed through the water-in-oil microemulsion procedure with an aim to reveal the potential of the amino-modified SNs in deposition of $[\{Re_6S_8\}(OH)_6]^{4-}$. The procedure was optimized for synthesis of 52.5 ± 3 nm sized $SNsNH_2$ (Fig. 1a), where both size and surface decoration by amino-groups (3200 per each $SNsNH_2$) (Fig. S1) are prerequisite for convenient cell internalization. The deposition of $[\{Re_6S_8\}(OH)_6]^{4-}$ cluster onto amino-decorated silica surface of $SNsNH_2$ is driven by their electrostatic attraction to the oppositely charged ammonium groups, although the extraction of the cluster units at $SNsNH_2$ requires greater time than that of $\{Mo_6I_8\}$-based anionic clusters [14] (for more details see the Exp. Section). The extraction is manifested by the decreased intensities of both electronic absorption and emission spectra of the clusters in the supernatant solutions (Fig. S2a, b). The quantitative analysis of the spectra (Fig. S2) indicates that 0.0175 mM of $[\{Re_6S_8\}(OH)_6]^{4-}$ are extracted by 0.5 $g{\cdot}L^{-1}$ of $SNsNH_2$. The spectra of the supernatants after washing of the separated nanoparticulate phase indicate insignificant leaching of the cluster. The separated phase can be easily redispersed in aqueous solutions. The composition of the nanoparticulate phase was evaluated by means of the Si:Re molar ratios (Table 1) calculated from the ICP-OES analysis (Table S1). The composite SNs in Table 1 and further are designated as $[Re_6]$-$SNsNH_2$. Both polydispersity index (PDI) values and average size of aggregates are smaller for $[Re_6]$-$SNsNH_2$ than those of $SNsNH_2$ (Table 1). The large difference in electron density between the $\{Re_6S_8\}^{2+}$ cluster core and $Si\text{-}O^-$ from the silica matrix facilitates the recognition of the cluster units at the spheres. Indeed, the TEM images of $[Re_6]$-$SNsNH_2$ (Fig. 1b) reveal the outgrowths at the amino-modified silica surface. The uniform coating of the nanoparticles by the outgrowths confirms the exterior deposition of $[\{Re_6S_8\}(OH)_6]^{4-}$.

Literature data represent the adsorption of PEI onto the surface of naked SNs as the efficient non-covalent surface decoration [13], while the surface exposed amino- and ammonium groups are the prerequisite for the deposition of the cluster units. The naked SNs with the average size of 43.2 ± 2 nm were synthesized by the similar microemulsion procedure (Fig. 1c). The PEI adsorption on the naked SNs was performed by their mixing with the aqueous solution of PEI and further phase separation of the nanoparticulate phase (for more details see the Experimental Section). The electrokinetic potential values of the naked SNs revealed efficient recharging from −44 to +44 mV after the adsorption of PEI (Table 1). The PEI-treated SNs will be further designated as PEI-SNs. The PEI-SNs are manifested by the enhanced stability to aggregation in comparison with $SNsNH_2$ (Table 1). This fact derives from the formation of the highly hydrated PEI-based exterior layer [13], which provides a basis for further deposition of the anionic cluster units. The recharged SNs were deposited by the anionic cluster units by means of the similar procedure (for more details see the Exp. Section).

The analysis of the UV-Vis and luminescence spectra in the initial and supernatant solutions (Fig. S2a, b) indicates that similar with the amino-decorated SNs the PEI-deposited SNs (0.5 g L^{-1}) extract 0.0175 mM of $[\{Re_6S_8\}(OH)_6]^{4-}$. The ICP-OES analysis confirms the similarity in the Si:Re ratios for $[Re_6]$-$SNsNH_2$ and $[Re_6]$-PEI-SNs (Tables 1 and S1). $[Re_6]$-PEI-SNs in the TEM images (Fig. 1d) are manifested as the spheres coated by the brighter exterior layer (about 5.3 nm thickness), while the deposited cluster complexes are revealed by the dark spots in the TEM image (Fig. 1d).

The previously reported doping procedure [15] was also applied as an alternative way of the incorporation of the cluster units into SNs. The reported procedure was modified by increasing of the cluster-to-TEOS ratio in order to get the composite SNs with the Si:Re ratio close to the values achieved for $[Re_6]$-PEI-SNs and $[Re_6]$-$SNsNH_2$. The Si:Re ratio revealed by ICP-OES analysis was 1:0.014, which confirmed the composite nature of the nanoparticles designated as $[Re_6]$@$SNsNH_2$. The TEM images of $[Re_6]$@$SNsNH_2$ reveal their size greater than 100 nm, while the cluster units are manifested by the dark rods or globules inside the composite SNs (Fig. 1e). The X-ray diffraction pattern (XRD) of $[Re_6]$@$SNsNH_2$ (Fig. S3) confirms nanocrystalline inclusions of the cluster manifested by the peak in the region of smaller angles additional to the broad peak arising from amorphous silica (Fig. S3). The presented in Fig. S3 XRD pattern of "empty" SNs reveals the amorphous silica without polycrystalline inclusions. The difference in electronic densities of the cluster units and silica coating enables to evaluate the former by SAXS analysis, while exterior size of $[Re_6]$@$SNsNH_2$ lies above the values available for correct evaluation by

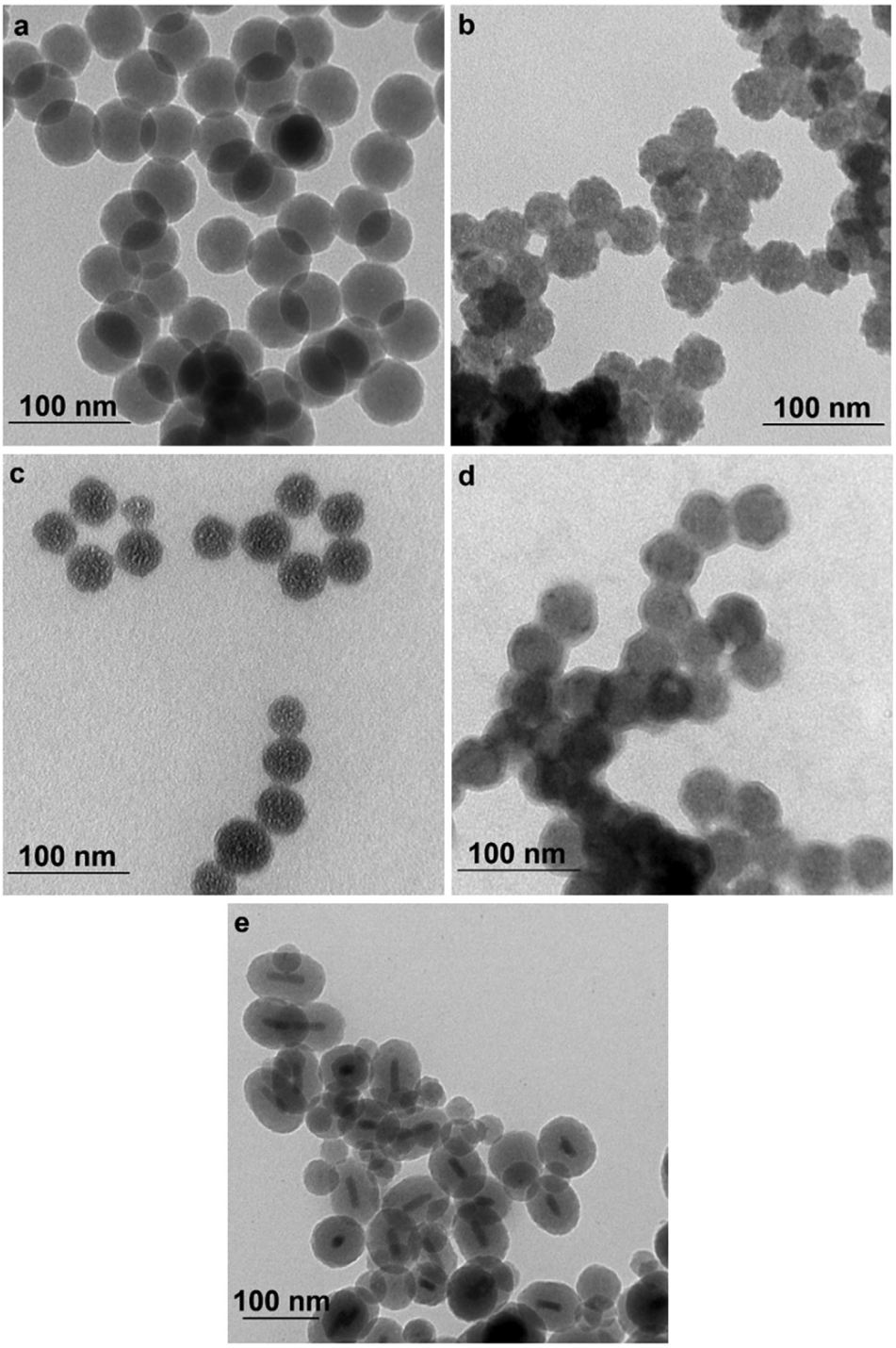

Fig. 1. The TEM images of $SNsNH_2$ (a), $[Re_6]$-$SNsNH_2$ (b), SNs (c), $[Re_6]$-PEI-SNs (d), and $[Re_6]$@$SNsNH_2$ (e).

Table 1
Average size (d_{DLS} and d_{TEM}), electrokinetic potentials (ζ_{DLS}) values, polydispersity indexes (PDI_{DLS}) and the Si:Re molar ratios determined by ICP-EOS of the differently synthesized composite SNs in aqueous solution, C_{SNs} = 0.1 $g{\cdot}L^{-1}$.

Type of silica particles	d_{DLS}, nm	PDI_{DLS}	ζ_{DLS}, mV	d_{TEM}, nm	Si:Re
$SNsNH_2$	aggregation	0.673	+23 ± 3	52.5 ± 3	–
$[Re_6]$-$SNsNH_2$	151 ± 1	0.348	+10 ± 1	52.5 ± 3	1:0.027
SNs	131 ± 0.1	0.102	−44 ± 2	43.2 ± 2	–
PEI-SNs	142 ± 0.35	0.116	+44 ± 1	–	–
$[Re_6]$-PEI-SNs	318 ± 5	0.431	+39 ± 0.4	54 ± 3	1:0.026
$[Re_6]$@$SNsNH_2$	aggregation	0.665	+27 ± 0.5	89(±10)× ×69(±3) 45 ± 9	1:0.014

the method (1–60 nm). The SAXS data are represented in Fig. S4. Table 2 collects the calculated from the SAXS data parameters characterizing nanoparticles, such as radius of gyration (R_g and R_g^*) evaluated by Guinier method and from analysis of distance distribution function respectively, biggest distances in the particles (D_{max}) and average diameter of the particles calculated in a sphere-shaped model framework (d_s, $d_s = 2\sqrt{((5/3)\cdot R_g^2)}$). The d_s-values calculated for $[Re_6]$@$SNSNH_2$ refer to the average size of the polycrystalline inclusions. For comparison the SAXS data were also measured for $[Re_6]$-$SNSNH_2$ and $[Re_6]$-PEI-SNs (Fig. S4). The d_s-values calculated for these SNs are smaller than the sizes revealed by the TEM images (Fig. 1, Table 1). The deviation between d_s and d_{TEM} values is common for SNs, since it derives from the difference in the electronic densities in the core and shell zones of SNs.

3.2. Spectral properties of the cluster units in composite SNs

It is worth mentioning the work [34] for highlighting the pH-dependent spectral properties of $[\{Re_6S_8\}(OH)_6]^{4-}$. It is, in particular, well-known that the cluster exists in its hexahydroxo form ($[\{Re_6S_8\}(OH)_6]^{4-}$) in alkaline conditions at pH above 10.0, which is characterized by the peculiar ratio of the absorbance values measured at 360 and 416 nm (A_{360}/A_{416}). The step-wise protonation of the apical hydroxo ligands of the cluster at pHs below 10.0 represented by the Eq. (1) is followed by the changes in the electronic absorption spectra demonstrated in Fig. 2a. The pH-induced changes of A_{360}/A_{416} plotted in Fig. 2b indicates that the protonation of the apical hydroxo ligands of the cluster complex is significantly restricted in the presence of PEI. This specific behavior of the cluster units derives from their interaction with amino/ammonium groups of PEI chains.

$$\left[\{Re_6S_8\}(OH)_6\right]^{4-} + xH^+ = \left[\{Re_6S_8\}(H_2O)_x\left(OH\right)_{(6-x)}\right]^{(x-4)} \quad (1)$$

Unfortunately, the spectral profile of the cluster units can't be monitored from the UV-Vis spectra of $[Re_6]$-PEI-SNs and $[Re_6]$-$SNSNH_2$ (Fig. S5) due to the interference of the cluster-centered absorbance with the scattering effect arisen from the silica nanobeads. Nevertheless, similar with PEI, the amino/ammonium groups of both PEI-SNs and $SNSNH_2$ should provide the similar shifting of the equilibrium (1).

The luminescence intensity of the cluster complex in aqueous solution comes to the low level even within three days of storage (Fig. S6), while that of $[Re_6]$-PEI, $[Re_6]$-$SNSNH_2$ or $[Re_6]$-PEI-SNs remains enough high within 25 days at least (Fig. S6). This indicates that the degradation of the clusters is significantly slowed down under their wrapping by PEI chains or incorporation into the nanoparticulate forms.

It is also worth noting that both wrapping by PEI chains of the cluster units and their adsorption at the surfaces of $SNSNH_2$ and PEI-SNs result in the enhancement of the cluster-centered luminescence (Fig. 3). The excited state lifetime values (τ) determined for the cluster complexes in the molecular and nanoparticulate forms at various pHs are presented in Table 3. The τ-values at neutral pH are in the following order: $[Re_6]$-PEI-SNs $\approx$ $[Re_6]$-PEI > $[Re_6]$-$SNSNH_2$ > $[\{Re_6S_8\}(OH)_6]^{4-}$ (Table 3). It is worth correlating the τ-values with an extent of radiationless decay of the cluster's excited state in aqueous oxygenated solutions. Thus, the wrapping capacity of PEI-chains in both $[Re_6]$-PEI-SNs and $[Re_6]$-PEI provides more efficient shielding of the clusters from an oxygenation than the surface exposed amino-groups in $[Re_6]$-$SNSNH_2$.

The Si:Re ratio for $[Re_6]$@$SNSNH_2$ is of the same order of magnitude with the ratios evaluated for $[Re_6]$-$SNSNH_2$ and $[Re_6]$-PEI-SNs (Tables 1 and S1). However, the emission intensity of $[Re_6]$@$SNSNH_2$ is weak at the similar equipment and concentration conditions and thus is not represented herein. Thus, the incorporation of the cluster units into the core zone of the silica nanobeads doesn't provide any potential for an applicability of the cluster-centered luminescence in sensing or imaging.

The aforesaid results highlight the interaction of the cluster units with amino/ammonium groups as the reason for both shifting of the equilibrium (1) and restricted radiationless decay due to the wrapping effect of PEI. However, the ability of PEI chains to wrap around the anionic cluster units depends on the ratio of amino-to-ammonium groups which, in turn, is pH-dependent. The luminescence spectra of $[Re_6]$-PEI-SNs and $[Re_6]$-$SNSNH_2$, along with $[\{Re_6S_8\}(OH)_6]^{4-}$ and $[Re_6]$-PEI measured at pH from 4.0 to 9.0 are presented in Fig. 3, while those recorded at pH from 9.0 to 12.0 are in Fig. S6. The luminescence intensities at 615 nm are plotted versus pHs in Fig. 4a in order to compare the pH-dependencies for different molecular or nanoparticulate forms of the cluster. The pH-dependencies of emission intensities are pronounced and similar for $[Re_6]$-PEI and $[Re_6]$-PEI-SNs, while the luminescence spectrum of $[Re_6]$-$SNSNH_2$ exhibits very poor changes under pH variation (Fig. 3c and 4a). The aforesaid tendencies are quite different from that for $[\{Re_6S_8\}(OH)_6]^{4-}$ (Fig. 4a), where the pH-decrease from 12.0 to 4.0 results in the pronounced intensity changes of $[\{Re_6S_8\}(OH)_6]^{4-}$ derived from its step-wise protonation due to the equilibrium (1).

The pH-induced transformation of amino-to-ammonium groups at the silica/water interface was followed by electrokinetic potential (ζ) measurements for $SNSNH_2$ and $[Re_6]$-$SNSNH_2$, as well as for PEI-SNs and $[Re_6]$-PEI-SNs. The ζ-values at different pHs are plotted in Fig. 4b for correlation with the pH-dependent luminescence shown in Fig. 4a. The negative ζ-values of $SNSNH_2$ at pH > 10.0 refer to low ammonium-to-amino groups ratio, while the increase in the ζ-values at 4 < pH < 10 results from the amino-to-ammonium groups conversion (Fig. 4b). The luminescence of $[\{Re_6S_8\}(OH)_6]^{4-}$ is insignificantly influenced by $SNSNH_2$ at pH > 10.0 due to the low amount of ammonium groups at the surface (Fig. 4a). The growing amount of the ammonium groups at 4 < pH < 10 should enhance the electrostatic attraction of $[\{Re_6S_8\}(OH)_6]^{4-}$ anions with $SNSNH_2$. Thus, the invariant luminescence of $[Re_6]$-$SNSNH_2$ at 4 < pH < 10 indicates that the protonation of $[\{Re_6S_8\}(OH)_6]^{4-}$ units is restricted due to their extra-stabilization through the binding with the ammonium groups (Fig. 4a). This tendency differentiates $[Re_6]$-$SNSNH_2$ from $[Re_6]$-PEI-SNs and $[Re_6]$-PEI, where protonation of PEI under the pH-decrease from 11.0 to 8.0 results in the enhancement of the cluster-centered luminescence which comes to the saturation level at pH 8.0–6.0 (Fig. 3b, d and 4a). The changes in the luminescence correlates with the partial protonation of PEI, which is followed by the growing capacity of PEI chains to wrap around the cluster units due to favoring of their coil-like conformation [43]. Thus, both enhanced level of the cluster-centered luminescence and its invariance at pH 8.0–6.0 result from the wrapping of the cluster units by PEI.

Table 2
The R_g, R_g^*, D_{max}, d_s, and V_{part} (averaged particle volume) values, the scattering intensity at s = 0 (I_0, in arbitrary units) of $[Re_6]$@$SNSNH_2$, $[Re_6]$-$SNSNH_2$, and $[Re_6]$-PEI-SNs.

Type of silica particles	R_g, Å	R_g^*, Å	D_{max}, nm	V_{part}, Å^3	I_0, a.u.	d_s, nm
$[Re_6]$@$SNSNH_2$	148.7	148.8	48.1	$144\cdot10^5$	216,900	38.4
$[Re_6]$-$SNSNH_2$	128.9	128.8	41.6	$109\cdot10^5$	170,000	33.3
$[Re_6]$-PEI-SNs	133.6	133.5	40.9	$122\cdot10^5$	179,900	34.5

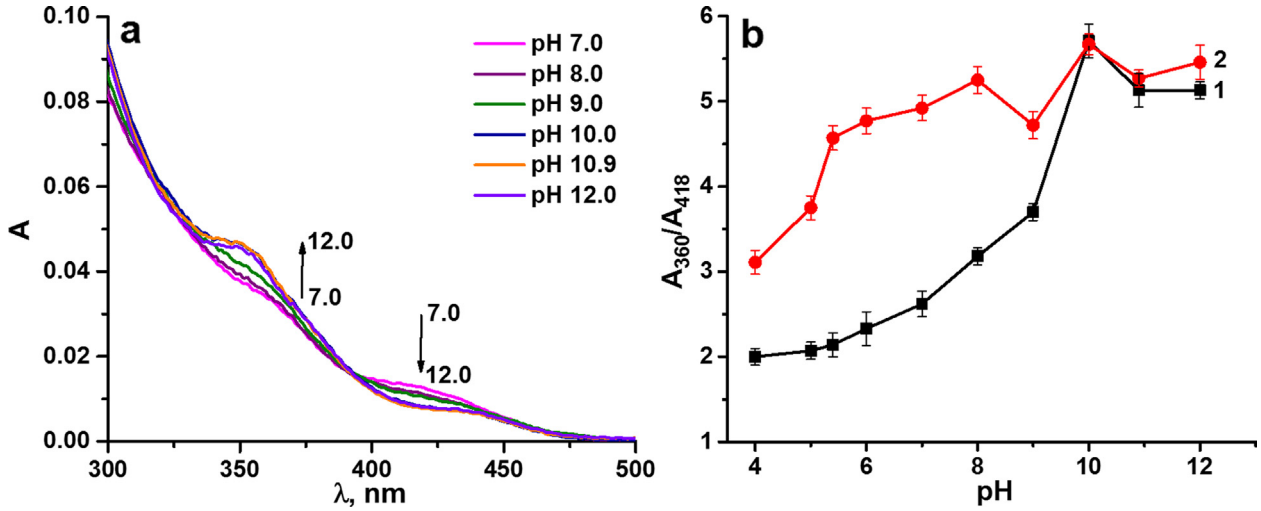

Fig. 2. Electronic absorption spectra of $[\{Re_6S_8\}(OH)_6]^{4-}$ (a) and A_{360}/A_{418} values (b) of $[\{Re_6S_8\}(OH)_6]^{4-}$ (**1**) and $[Re_6]$-PEI (**2**) at various pH values ($C_{Cluster}$ = 0.0175 mM, C_{PEI} = 0.0175 mM). The SD values are designated by error bars.

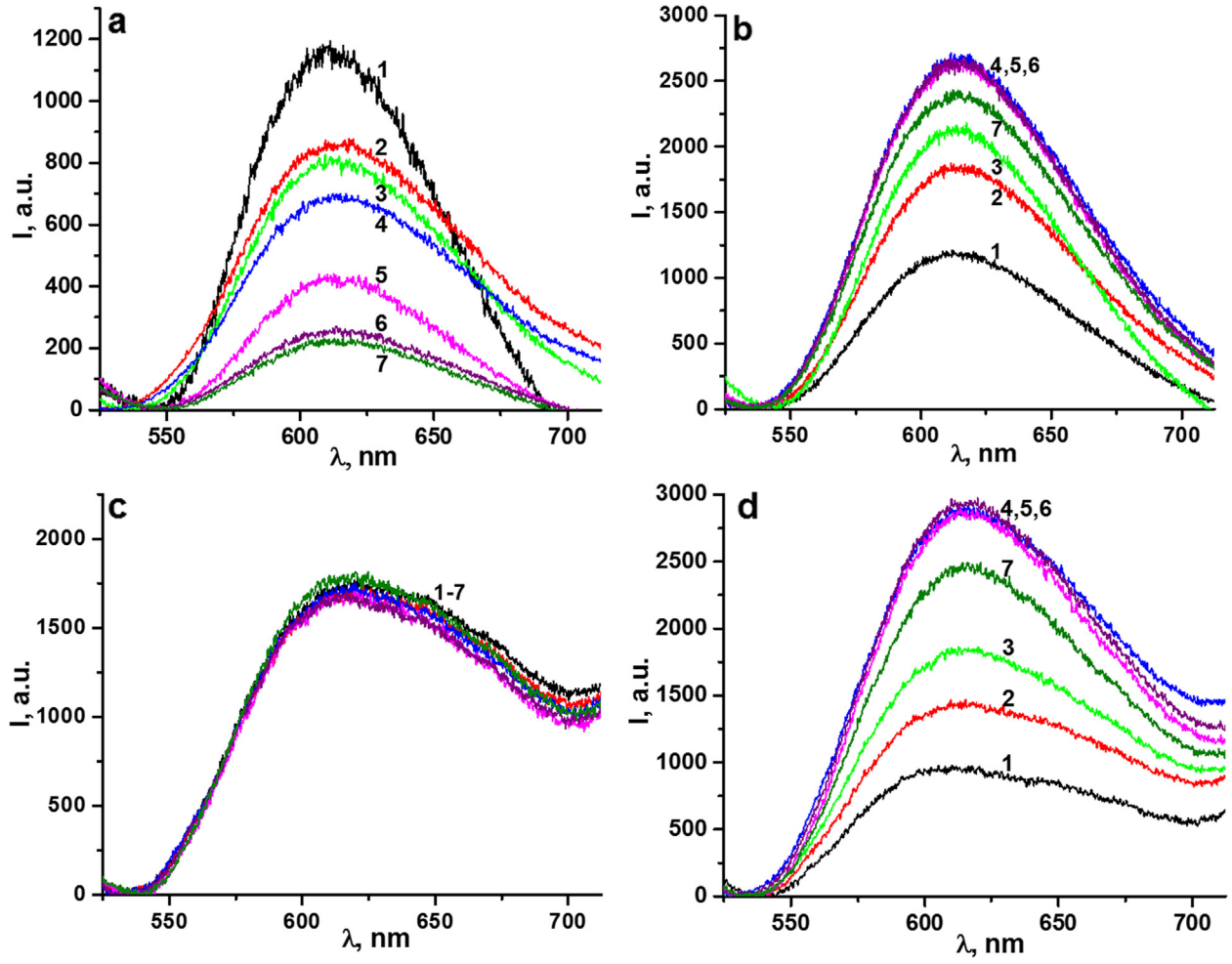

Fig. 3. Luminescence spectra of $[\{Re_6S_8\}(OH)_6]^{4-}$ (a), $[Re_6]$-PEI (b), $[Re_6]$-$SNsNH_2$ (c), and $[Re_6]$-PEI-SNs (d) at various pH values – 4.0 (**1**), 5.0 (**2**), 5.4 (**3**), 6.0 (**4**), 7.0 (**5**), 8.0 (**6**), and 9.0 (**7**) ($C_{Cluster}$ = 0.0175 mM, C_{PEI} = 0.0175 mM, C_{SNs} = 0.5 g·L^{-1}, λ_{ex} = 370 nm).

The sharp decrease of the luminescence intensities under the pH decrease from 6.0 to 4.0 (Fig. 4a) correlates with the documented in literature conformation changes of PEI from coil-to-linear when pH is decreased from 6.0 to 4.0 [43,44]. The conformational changes are driven by the interchain electrostatic repulsion of the ammonium groups resulted from the pH-induced protonation of PEI. Taking into account the impact of the coil-conformation on the wrapping of the cluster units by PEI

Table 3
The excited state lifetime values (τ) of $[\{Re_6S_8\}(OH)_6]^{4-}$, $[Re_6]$-PEI, $[Re_6]$-$SNsNH_2$, and $[Re_6]$-PEI-SNs in aqueous solutions ($C_{Cluster}$ = 0.0175 mM, C_{PEI} = 0.0175 mM, C_{SNs} = 0.5 g·L^{-1}).

Sample	pH	$[\{Re_6S_8\}(OH)_6]^{4-}$	$[Re_6]$-PEI	$[Re_6]$-$SNsNH_2$	$[Re_6]$-PEI-SNs
τ, μs	4.0	7.15 ± 0.14	8.55 ± 0.09	8.43 ± 0.08	8.7 ± 0.12
	5.0	6.81 ± 0.14	9.82 ± 0.32	8.7 ± 0.11	9.36 ± 0.22
	5.4	6.77 ± 0.14	10.68 ± 0.42	8.71 ± 0.1	10.52 ± 0.34
	6.0	6.64 ± 0.16	10.62 ± 0.41	8.74 ± 0.11	10.42 ± 0.32
	7.0	5.58 ± 0.29	10.37 ± 0.39	8.71 ± 0.09	10.39 ± 0.32
	8.0	4.83 ± 0.31	10.4 ± 0.38	8.77 ± 0.11	10.67 ± 0.34
	9.0	5.08 ± 0.09	9.76 ± 0.3	9.06 ± 0.18	10.56 ± 0.36
	10.0	6.52 ± 0.31	9.93 ± 0.3	9.56 ± 0.27	9.98 ± 0.28
	10.9	7.32 ± 0.24	8.92 ± 0.16	9.68 ± 0.26	9.82 ± 0.25
	12.0	8.06 ± 0.14	9.07 ± 0.3	9.7 ± 0.31	9.09 ± 0.16

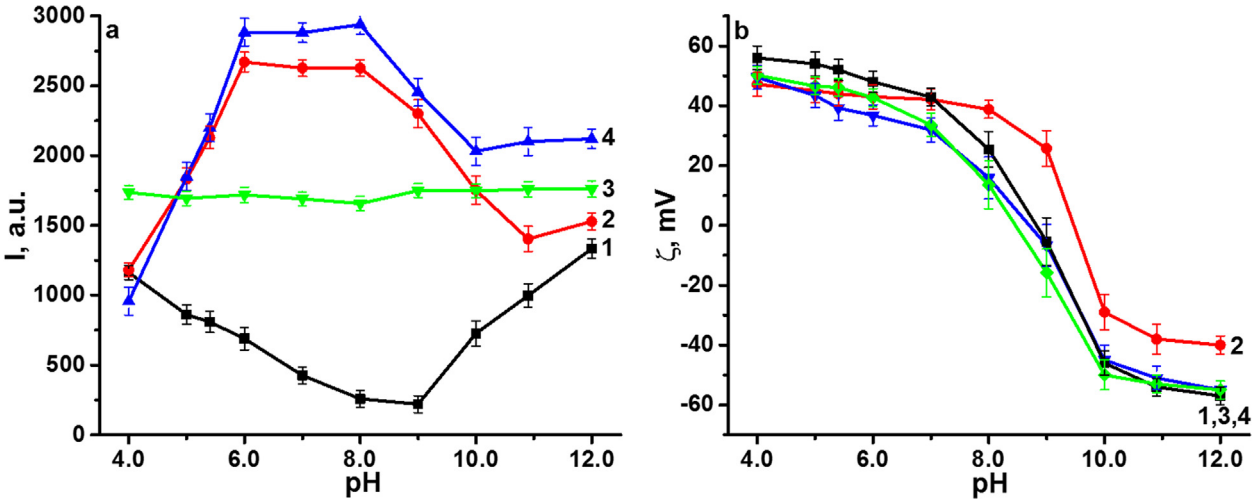

Fig. 4. (a) Luminescence intensity at 615 nm of $[\{Re_6S_8\}(OH)_6]^{4-}$ (**1**), $[Re_6]$-PEI (**2**), $[Re_6]$-$SNsNH_2$ (**3**), and $[Re_6]$-PEI-SNs (**4**) at various pH values ($C_{Cluster}$ = 0.0175 mM, C_{PEI} = 0.0175 mM, C_{SNs} = 0.5 g·L^{-1}, λ_{ex} = 370 nm); (b) Electrokinetic potential (ζ, mV) of $SNsNH_2$ (**1**), PEI-SNs (**2**), $[Re_6]$-$SNsNH_2$ (**3**), and $[Re_6]$-PEI-SNs (**4**) colloids at various pH values (C_{SNs} = 0.1 g·L^{-1}). The SD values are designated by error bars.

chains, their linearization should be followed by the unwrapping effect. Thus, the experimentally observed decrease in the luminescence intensities of $[Re_6]$-PEI-SNs and $[Re_6]$-PEI at 4.0 < pH < 6.0 (Fig. 4a) can be explained by the partial release of the cluster units from the PEI-based confinement. The aforesaid pH-induced intensity changes are followed by the decrease in the τ-values (Table 3) of $[Re_6]$-PEI and $[Re_6]$-PEI-SNs, although these values are still greater than τ-values of the naked cluster complex at the same pHs. This fact indicates that even unwrapped protonated PEI chains restrict the protonation of the cluster units due to their interaction with ammonium groups of PEI. The pH-triggered wrapping and unwrapping is illustrated by the cartoon image in Fig. 5.

Thus, the deposition of $[\{Re_6S_8\}(OH)_6]^{4-}$ onto $SNsNH_2$ is stable in the wide pH-range, while $[Re_6]$-PEI-SNs represents the pH-dependent deposition mode. The cytotoxicity and cell internalization of both nanoparticulate forms should be studied in order to recognize their applicability in cellular imaging or sensing.

3.3. Cytotoxicity and cell internalization of the composite SNs

It is worth discussing both literature and the experimental data on the cytotoxicity of building blocks belonging to the composite SNs before the presentation of their cytotoxicity. The low cytotoxicity of both $SNsNH_2$ and SNs is well-known [45], while the surface decoration by PEI can increase a cytotoxicity due to the cytotoxic effect of the latter [46]. However, the presented in Table 4 cell viability data reveal rather low cytotoxicity of PEI-SNs. The previously reported high IC_{50} values of $[\{Re_6S_8\}(OH)_6]^{4-}$ which are 0.262 mM for HeLa [26] and 0.366 mM for Hep-2 [36] agree well with the poor cellular uptake of the anionic cluster complex. The greater cell internalization of $[Re_6]$-PEI correlates with the higher cytotoxicity of the assembly (0.113 mM) reported for Hep-2 cells [36]. However, the embedding of the cluster units into the composite SNs can significantly affect their cytotoxic effect due to the difference in the cellular uptake mechanisms of molecular and nanoparticulate forms [47,48].

The cell viabilities measured at various concentrations of $[Re_6]$-PEI-SNs and $[Re_6]$-$SNsNH_2$ are presented in Table 4. The concentrations of the SNs are represented by the concentrations of both cluster units (mM) and the SNs (g·L^{-1}). The cell viability of Chang Liver cell line exhibits the detectable decrease after the incubation by the composite SNs at their greatest applied concentration (0.25 g·L^{-1}). However, the enhanced cell internalization of both nanoparticulate forms enables to get enough contrasting effect at the lower concentration (0.1 g·L^{-1}), which is demonstrated by flow cytometry data in Fig. 6. The results (Fig. 6) indicate that $[Re_6]$-PEI-SNs provide the better contrasting effect than $[Re_6]$-$SNsNH_2$.

The intracellular distribution of $[Re_6]$-PEI-SNs has been visualized by confocal microscopy images of M−HeLa cells incubated by the composite SNs (Fig. 7). The incubation of the cell samples by DAPI enables to stain by blue the cell nuclei (Fig. 7). This, in turn, reveals that staining by DAPI interferes with that by $[Re_6]$-PEI-SNs. Commonly, SNs tend to localize predominantly in the cell cytoplasm [45,49,50], thus, the reasons for the staining of the cell nuclei by $[Re_6]$-PEI-SNs is worth discussing.

Thus, $[Re_6]$-PEI-SNs after the efficient cell internalization are able to stain the cell nuclei, which points to their endosomal escape into the cytosol and traffic in close proximity to the nuclear pore complex [51]. It is worth noting that endocytosis mechanism of nanoparticles is greatly dependent on their size [16]. Thus, the

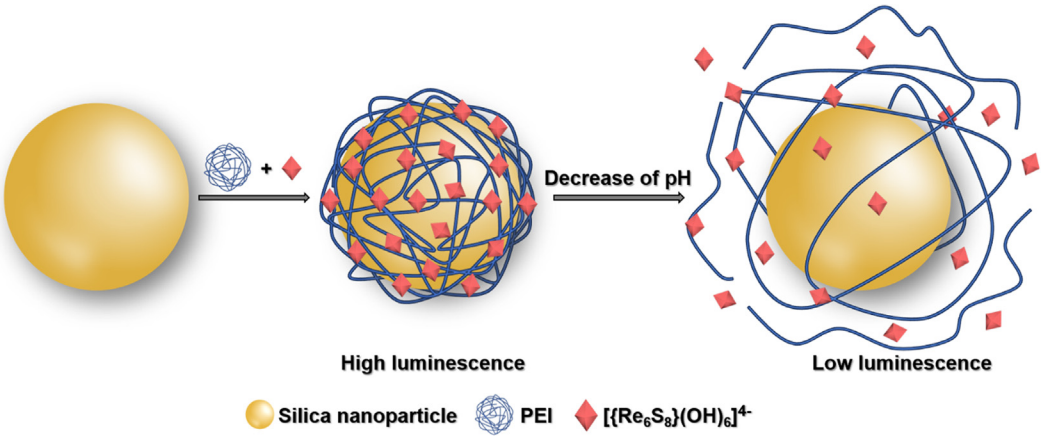

Fig. 5. Cartoon illustration of the pH-triggered wrapping and unwrapping of PEI chains as the reason for the pH-dependent cluster-centered luminescence.

Table 4
Cell viability of Chang Liver and M−HeLa cells incubated by $[Re_6]$-PEI-SNs and $[Re_6]$-$SNsNH_2$.

Sample	C_{SNs}, $g{\cdot}L^{-1}$	$C_{Cluster}$, mM	Cell viability, %	
			M−HeLa	Chang Liver
$[Re_6]$-PEI-SNs	0.25	0.00875	92.5	44.1
	0.125	0.00437	100	46
	0.0625	0.00219	100	95.8
	0.0313	0.0011	100	100
$[Re_6]$-$SNsNH_2$	0.25	0.00875	92.7	57.9
	0.125	0.00437	100	93.5
	0.0625	0.00219	100	100
PEI-SNs	1.25	–	80.8	90.3
	0.625	–	92.1	81.5
	0.3125	–	94.1	89.8
	0.156	–	97.0	95.6
	0.078	–	96.7	96.4
	0.039	–	96.2	97.7

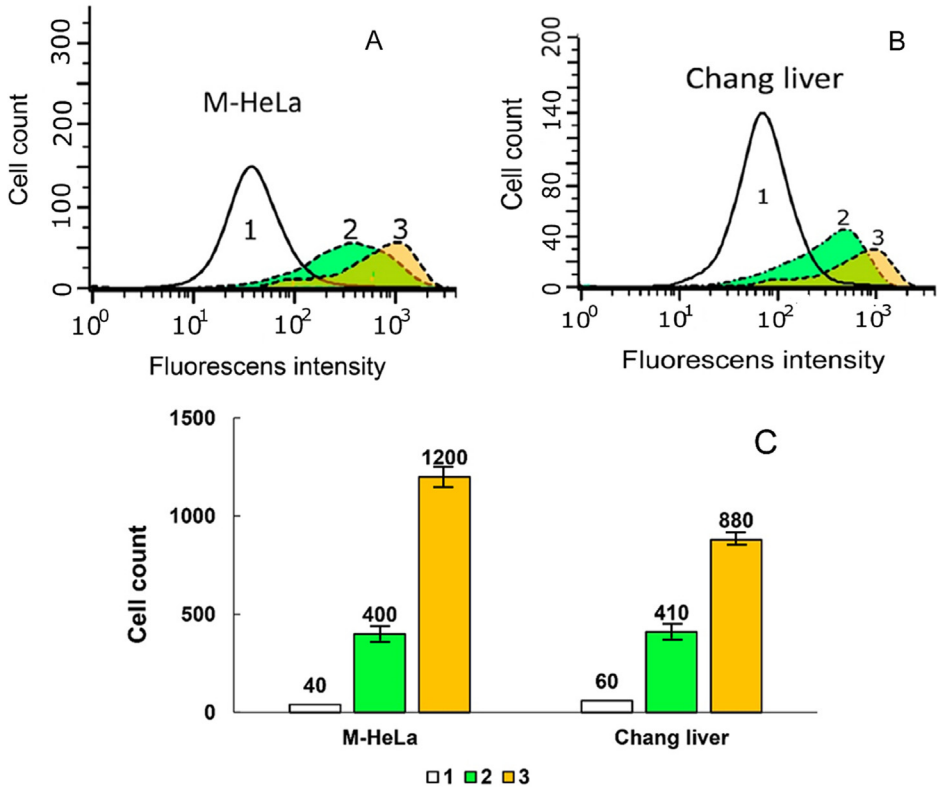

Fig. 6. Flow cytometry data (A, B) for $[Re_6]$-$SNsNH_2$ (**2**) and $[Re_6]$-PEI-SNs (**3**): luminescence intensity of M−Hela (**1**, A) and Chang Liver (**1**, B) cells (control), after the incubation for 24 h with $[Re_6]$-$SNsNH_2$ (**2**) and $[Re_6]$-PEI-SNs (**3**) (C_{SNs} = 0.1 $g{\cdot}L^{-1}$); (C) Mean fluorescence intensity from the flow cytometry histograms shown as a function of the nanoparticles type. The SD values are designated by error bars.

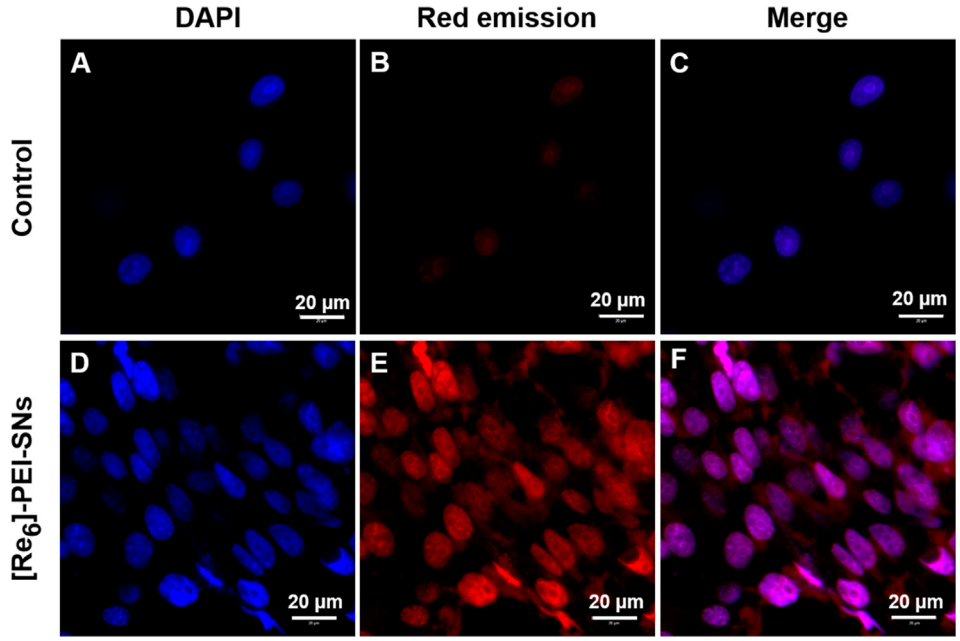

Fig. 7. Confocal fluorescent laser microscopy images of control M−HeLa cell lines (A, B, C) and M−HeLa cells incubated with $[Re_6]$-PEI-SNs (D, E, F).

size of $[Re_6]$-PEI-SNs being about 50 nm (Table 1) indicates that their cell internalization into M−HeLa cells can be driven by both clathrin-dependent and caveolin-mediated mechanisms of endocytosis [52]. Important to note that the caveolin-mediated endocytosis is reported in literature [51] as one of the factors facilitating the release of nanoparticles from endosome confinement. In turn, nucleocytoplasmic transport is mediated by nuclear pore complexes that are 60-nm-diameter channels in the nuclear envelope, which encloses the nucleus from the cytoplasm [53]. Thus, the size of $[Re_6]$-PEI-SNs being below 60 nm could also be important to bypass nuclear pore complex to release from cytoplasm into the nuclear interior. For the best of our knowledge the present results for the first time highlight the optimal nanoarchitecture of nanoparticles able to deliver the anionic cluster units to cell nuclei for their efficient staining by the red cluster-centered luminescence.

4. Conclusions

Summarizing, the results highlight the supramolecular assembly of the anionic cluster complex $[\{Re_6S_8\}(OH)_6]^{4-}$ at silica nanoparticles (SNs) through the surface exposed amino-ammonium groups as the route for developing of both pH-sensitive and pH-insensitive cellular contrast agents with red cluster-centered luminescence. The pH-insensitive cellular contrast agents result from the efficient electrostatically driven assembly of $[\{Re_6S_8\}(OH)_6]^{4-}$ with amino-ammonium groups arisen from their covalent embedding onto the surface of amino-decorated SNs ($SNsNH_2$). The self-assembly of polyethyleneimine (PEI) chains at the negative surface of SNs forms the positively charged exterior layer (PEI-SNs) with the surface exposed amino-ammonium groups. The flexibility of PEI chains results in unique wrapping-like binding mode of the cluster units manifested by the pronounced enhancement of their luminescence in comparison with the "free" cluster complex in aqueous solutions. $[\{Re_6S_8\}(OH)_6]^{4-}$ deposited onto PEI-SNs exhibits the pronounced decrease in the steady state and time resolved cluster-centered luminescence under the acidification within pH range from 6.0 to 4.0 due to the pH-driven conformational changes of PEI chains.

The deposition of $[\{Re_6S_8\}(OH)_6]^{4-}$ onto PEI-SNs makes these nanoparticles better cellular contrasting agents versus those deposited onto $SNsNH_2$. Moreover, the embedding of the cluster units onto PEI-SNs provides the efficient staining of the cell nuclei demonstrated for M−HeLa cell line. It is also worth noting that the staining of the cell nuclei by red luminescence of $[Re_6]$-PEI-SNs highlights the route for deliverance of polyanions to cell nuclei. The revealed herein nuclear localization of $[Re_6]$-PEI-SNs opens the ways beyond specific peptides [54] to achieve target binding of composite SNs with cell nuclei. The pH-sensitive luminescence of $[Re_6]$-PEI-SNs opens their future in sensing of early-to-late endosome conversion as the prerequisite of endosomal escape and entering cell nuclei.

CRediT authorship contribution statement

Alsu Khazieva: Methodology, Formal analysis, Investigation, Writing - original draft, Writing - review & editing. **Kirill Kholin:** Formal analysis. **Irek Nizameev:** Formal analysis. **Konstantin Brylev:** Resources, Investigation, Writing - review & editing. **Ilya Kashnik:** Resources, Investigation. **Alexandra Voloshina:** Formal analysis, Investigation. **Anna Lyubina:** Formal analysis, Investigation. **Aidar Gubaidullin:** Formal analysis, Investigation. **Amina Daminova:** Formal analysis, Investigation. **Konstantin Petrov:** Formal analysis, Writing - review & editing. **Asiya Mustafina:** Conceptualization, Writing - original draft, Writing - review & editing.

Declaration of Competing Interest

The authors declare that they have no known competing financial interests or personal relationships that could have appeared to influence the work reported in this paper.

Acknowledgements

The authors gratefully acknowledge the Assigned Spectral-Analytical Center of FRC Kazan Scientific Center of RAS. The authors

thank to Interdisciplinary Center for Analytical Microscopy at KFU for assistance with the confocal microscopy experiments.

The work was funded by the Government assignment for FRC Kazan Scientific Center of Russian Academy of Science (Reg. Nr. AAAA-A18-118041760011-2).

Appendix A. Supplementary data

Supplementary data to this article can be found online at https://doi.org/10.1016/j.jcis.2021.03.082.

References

[1] J. Feng, J. Yang, Y. Shen, W. Deng, W. Chen, Y. Ma, Z. Chen, S. Dong, Mesoporous silica nanoparticles prepared via a one-pot method for controlled release of abamectin: Properties and applications, Microporous Mesoporous Mater. 311 (2021) 110688.

[2] P. Jänicke, C. Lennicke, A. Meister, B. Seliger, L.A. Wessjohann, G.N. Kaluđerović, Fluorescent spherical mesoporous silica nanoparticles loaded with emodin: Synthesis, cellular uptake and anticancer activity, Mater. Sci. Eng., C 119 (2021) 111619.

[3] S. Ghosh, S. Dutta, A. Sarkar, M. Kundu, P.C. Sil, Targeted delivery of curcumin in breast cancer cells via hyaluronic acid modified mesoporous silica nanoparticle to enhance anticancer efficiency, Colloids Surf. B 197 (2021) 111404.

[4] J. Wang, Z. Li, Y. Yin, H. Liu, G. Tang, Y. Ma, X. Feng, H. Mei, J. Bi1, K. Wang, Z. Chen, Mesoporous silica nanoparticles combined with MoS2 and FITC for fluorescence imaging and photothermal therapy of cancer cells, J. Mater. Sci. 55 (2020) 15263–15274.

[5] R. Sakhtianchi, B. Darvishi, Z. Mirzaie, F. Dorkoosh, S. Shanehsazzadeh, R. Dinarvand, Pegylated magnetic mesoporous silica nanoparticles decorated with AS1411 Aptamer as a targeting delivery system for cytotoxic agents, Pharm. Dev. Technol. 24 (2019) 1063–1075.

[6] W. Donga, J. Wen, Y. Li, C. Wanga, S. Sun, D. Shang, Targeted antimicrobial peptide delivery in vivo to tumor with near infrared photoactivated mesoporous silica nanoparticles, Int. J. Pharm. 588 (2020) 119767.

[7] J. Li, Z. Ding, Y. Li, J. Miao, W. Wang, K. Nundlall, S. Chen, Reactive oxygen species-sensitive thioketal-linked mesoporous silica nanoparticles as drug carrier for effective antibacterial activity, Mater. Des. 195 (2020) 109021.

[8] Y. Umehara, Y. Kimura, F. Kleitz, T. Nishihara, T. Kondo, K. Tanabe, Phosphonated mesoporous silica nanoparticles bearing ruthenium complexes used as molecular probes for tracking oxygen levels in cells and tissues, RSC Adv. 11 (2021) 5865–5873.

[9] J. Nayeem, Md.A.A. Al-Bari, Md. Mahiuddin, Md.A. Rahman, O.T. Mefford, H. Ahmad, Md.M. Rahman, Silica coating of iron oxide magnetic nanoparticles by reverse microemulsion method and their functionalization with cationic polymer P(NIPAm-co-AMPTMA) for antibacterial vancomycin immobilization, Colloids Surf. A 611 (2021) 125857.

[10] C. Guo, Y. Zhang, Y. Li, L. Zhang, H. Jiang, J. Tao, J. Zhu, Gold nanoparticle-guarded large-pore mesoporous silica nanocomposites for delivery and controlled release of cytochrome c, J. Colloid Interface Sci. 589 (2021) 34–44.

[11] J.A. Flood-Garibay, M.A. Méndez-Rojas, Synthesis and characterization of magnetic wrinkled mesoporous silica nanocomposites containing Fe_3O_4 or $CoFe_2O_4$ nanoparticles for potential biomedical applications, Colloids Surf. A 615 (2021) 126236.

[12] A.S. Taleghani, A.T. Nakhjiri, M. Khakzad, S.M. Rezayat, P. Ebrahimnejad, A. Heydarinasab, A. Akbarzadeh, A. Marjani, Mesoporous silica nanoparticles as a versatile nanocarrier for cancer treatment: A review, J. Mol. Liq. 328 (2021) 115417.

[13] N. Davydov, A. Mustafina, V. Burilov, E. Zvereva, S. Katsyuba, L. Vagapova, A. Konovalov, I. Antipin, Complex Formation of d-Metal Ions at the Interface of Tb^{III}-Doped Silica Nanoparticles as a Basis of Substrate-Responsive Tb^{III}-Centered Luminescence, ChemPhysChem 13 (2012) 3357–3364.

[14] J. Elistratova, A. Mukhametshina, K. Kholin, I. Nizameev, M. Mikhailov, M. Sokolov, R. Khairullin, R. Miftakhova, G. Shammas, M. Kadirov, K. Petrov, A. Rizvanov, A. Mustafina, Interfacial uploading of luminescent hexamolybdenum cluster units onto amino-decorated silica nanoparticles as new design of nanomaterial for cellular imaging and photodynamic therapy, J. Colloid Interface Sci. 538 (2019) 387–396.

[15] S. Fedorenko, J. Elistratova, A. Stepanov, A. Khazieva, M. Mikhailov, M. Sokolov, K. Kholin, I. Nizameev, R. Mendes, M. Rümmelid, T. Gemming, B. Weise, L. Giebeler, D. Mikhailova, S. Dutz, D. Zahn, A. Voloshina, A. Sapunova, A. Daminova, S. Fedosimova, A. Mustafina, ROS-generation and cellular uptake behavior of amino-silica nanoparticles arisen from their uploading by both iron-oxides and hexamolybdenum clusters, Mater. Sci. Eng., C 117 (2020) 111305.

[16] T. Bus, A. Traeger, Ulrich S. Schubert, The great escape: how cationic polyplexes overcome the endosomal barrier, J. Mater. Chem. B 6 (2018) 6904–6918.

[17] I.M.S. Degors, C. Wang, Z.U. Rehman, I.S. Zuhorn, Carriers Break Barriers in Drug Delivery: Endocytosis and Endosomal Escape of Gene Delivery Vectors, Acc. Chem. Res. 52 (2019) 1750–1760.

[18] R. Halaby, Role of lysosomes in cancer therapy, Res. Rep. Biol. 6 (2015) 147–155.

[19] T. Aubert, A.Y. Ledneva, F. Grasset, K. Kimoto, N.G. Naumov, Y. Molard, N. Saito, H. Haneda, S. Cordier, Synthesis and Characterization of $A_4[Re_6Q_8L_6]$ @SiO_2 Red-Emitting Silica Nanoparticles Based on Re_6 Metal Atom Clusters (A = Cs or K, Q = S or Se, and L = OH or CN), Langmuir 26 (2010) 18512–18518.

[20] N.A. Vorotnikova, A.Y. Alekseev, Y.A. Vorotnikov, V. Evtushok, Y. Molard, M. Amela-Cortes, S. Cordier, A.I. Smolentsev, C.G. Burton, P.M. Kozhin, P. Zhu, P.D. Topham, Y.V. Mironov, M. Bradley, O.A. Efremova, M.A. Shestopalov, Octahedral molybdenum cluster as a photoactive antimicrobial additive to a fluoroplastic, Mater. Sci. Eng., C 105 (2019) 110150.

[21] E. Rojas-Mancilla, A. Oyarce, V. Verdugo, Z. Zheng, R. Ramírez-Tagle, The Cluster $[Re_6Se_8I_6]^{3-}$ Induces Low Hemolysis of Human Erythrocytes in Vitro: Protective Effect of Albumin, Int. J. Mol. Sci. 16 (2015) 1728–1735.

[22] C. Falaise, A.A. Ivanov, Y. Molard, M. Amela Cortes, M.A. Shestopalov, M. Haouas, E. Cadota, S. Cordier, From supramolecular to solid state chemistry: Crystal engineering of luminescent materials by trapping molecular clusters in an aluminium-based host matrix, Mater. Horiz. 7 (2020) 2399–2406.

[23] N. Brandhonneur, Y. Boucaud, A. Verger, N. Dumait, Y. Molard, S. Cordier, G. Dollo, Molybdenum cluster loaded PLGA nanoparticles as efficient tools against epithelial ovarian cancer, Int. J. Pharm. 592 (2021) 120079.

[24] K. Kirakci, V. Šícha, J. Holub, P. Kubát, K. Lang, Luminescent Hydrogel Particles Prepared by Self-Assembly of β-Cyclodextrin Polymer and Octahedral Molybdenum Cluster Complexes, Inorg. Chem. 53 (2014) 13012–13018.

[25] A.O. Solovieva, K. Kirakci, A.A. Ivanov, P. Kubát, T.N. Pozmogova, S.M. Miroshnichenko, E.V. Vorontsova, A.V. Chechushkov, K.E. Trifonova, M.S. Fufaeva, E.I. Kretov, Y.V. Mironov, A.F. Poveshchenko, K. Lang, M.A. Shestopalov, Singlet Oxygen Production and Biological Activity of Hexanuclear Chalcocyanide Rhenium Cluster Complexes $[\{Re_6Q_8\}(CN)_6]^{4-}$ (Q = S, Se, Te), Inorg. Chem. 56 (2017) 13491–13499.

[26] S.-J. Choi, K.A. Brylev, J.-Z. Xu, Y.V. Mironov, V.E. Fedorov, Y.S. Sohn, S.-J. Kim, J.-H. Choy, Cellular uptake and cytotoxicity of octahedral rhenium cluster complexes, J. Inorg. Biochem. 102 (2008) 1991–1996.

[27] N. López-López, I. Muñoz Resta, R. de Llanos, J.F. Miravet, M. Mikhaylov, M.N. Sokolov, S. Ballesta, I. García-Luque, F. Galindo, Photodynamic Inactivation of Staphylococcus aureus Biofilms Using a Hexanuclear Molybdenum Complex Embedded in Transparent polyHEMA Hydrogels, ACS Biomater. Sci. Eng. 6 (2020) 6995–7003.

[28] A.O. Solovieva, Y.A. Vorotnikov, K.E. Trifonova, O.A. Efremova, A.A. Krasilnikova, K.A. Brylev, E.V. Vorontsova, P.A. Avrorov, L.V. Shestopalova, A. F. Poveshchenko, Y.V. Mironov, M.A. Shestopalov, Cellular internalisation, bioimaging and dark and photodynamic cytotoxicity of silica nanoparticles doped by $\{Mo_6I_8\}^{4+}$ metal clusters, J. Mater. Chem. B 4 (2016) 4839–4846.

[29] N.A. Vorotnikova, O.A. Efremova, A.R. Tsygankova, K.A. Brylev, M.V. Edeleva, O. G. Kurskaya, A.J. Sutherland, A.M. Shestopalov, Y.V. Mironov, M.A. Shestopalov, Characterization and cytotoxicity studies of thiol-modified polystyrene microbeads doped with $[\{Mo_6X_8\}(NO_3)_6]^{2-}$ (X = Cl, Br, I), Polym. Adv. Technol. 27 (2016) 922–928.

[30] A.M. Cheplakova, A.O. Solovieva, T.N. Pozmogova, Y.A. Vorotnikov, K.A. Brylev, N.A. Vorotnikova, E.V. Vorontsova, Y.V. Mironov, A.F. Poveshchenko, K.A. Kovalenko, M.A. Shestopalov, Nanosized mesoporous metal–organic framework MIL-101 as a nanocarrier for photoactive hexamolybdenum cluster compounds, J. Inorg. Biochem. 166 (2017) 100–107.

[31] E.V. Svezhentseva, A.O. Solovieva, Y.A. Vorotnikov, O.G. Kurskaya, K.A. Brylev, A.R. Tsygankova, M.V. Edeleva, S.N. Gyrylova, N. Kitamura, O.A. Efremova, M.A. Shestopalov, Y.V. Mironov, A.M. Shestopalov, Water-soluble hybrid materials based on $\{Mo_6X_8\}^{4+}$ (X = Cl, Br, I) cluster complexes and sodium polystyrene sulfonate, New J. Chem. 41 (2017) 1670–1676.

[32] K. Kirakci, T.K.N. Nguyen, F. Grasset, T. Uchikoshi, J. Zelenka, P. Kubát, T. Ruml, K. Lang, Electrophoretically Deposited Layers of Octahedral Molybdenum Cluster Complexes: A Promising Coating for Mitigation of Pathogenic Bacterial Biofilms under Blue Light, ACS Appl. Mater. Interfaces 12 (2020) 52492–52499.

[33] T. Hummel, D. Dutczak, A.Y. Alekseev, L.S. Adamenko, M.A. Shestopalov, Y.V. Mironov, D. Enseling, T. Jüstel, H.-J. Meyer, Photodynamic properties of tungsten iodide clusters incorporated into silicone: $A_2[M_6I_8L_6]$@silicone, RSC Adv. 10 (2020) 22257–22263.

[34] K.A. Brylev, Y.V. Mironov, S.S. Yarovoi, N.G. Naumov, V.E. Fedorov, S.-J. Kim, N. Kitamura, Y. Kuwahara, K. Yamada, S. Ishizaka, Y. Sasaki, A Family of Octahedral Rhenium Cluster Complexes $[Re_6Q_8(H_2O)_n(OH)_{6-n}]^{n-4}$ (Q = S, Se; n = 0–6): Structural and pH-Dependent Spectroscopic Studies, Inorg. Chem. 46 (2007) 7414–7422.

[35] J.G. Elistratova, A.R. Mustafina, K.A. Brylev, K.A. Petrov, M.A. Shestopalov, Y.V. Mironov, V.M. Babaev, I.K. Rizvanov, P. Masson, O.G. Sinyashin, Sensing activity of cholinesterases through a luminescence response of the hexarhenium cluster complex $[\{Re_6S_8\}(OH)_6]^{4-}$, Analyst 141 (2016) 4204–4210.

[36] J.G. Elistratova, K.A. Brylev, A.O. Solovieva, T.N. Pozmogova, A.R. Mustafina, L.V. Shestopalova, M.A. Shestopalov, V.V. Syakayev, A.A. Karasik, O.G. Sinyashin, Supporting effect of polyethylenimine on hexarhenium hydroxo cluster complex for cellular imaging applications, J. Photochem. Photobiol., A 340 (2017) 46–52.

[37] M. Kubeil, H. Stephan, H.-J. Pietzsch, G. Geipel, D. Appelhans, B. Voit, J. Hoffmann, B. Brutschy, Y.V. Mironov, K.A. Brylev, V.E. Fedorov, Sugar-Decorated Dendritic Nanocarriers: Encapsulation and Release of the

Octahedral Rhenium Cluster Complex $[Re_6S_8(OH)_6]^{4-}$, Chem. Asian J. 5 (2010) 2507–2514.
[38] S.S. Yarovoi, Y.V. Mironov, D.Y. Naumov, Y.V. Gatilov, S.G. Kozlova, S.-J. Kim, V. E. Fedorov, Octahedral hexahydroxo rhenium cluster complexes $[Re_6Q_8(OH)_6]^{4-}$ (Q = S, Se): Synthesis, structure, and properties, Eur. J. Inorg. Chem. 3945–3949 (2005).
[39] Y. Chen, Y. Zhang, Fluorescent quantification of amino groups on silica nanoparticle surfaces, Anal. Bioanal. Chem. 399 (2011) 2503–2509.
[40] Small Angle X-ray Scattering; Version 4.0; Software Reference Manual, M86-E00005-0600; Bruker AXS Inc.: Madison, WI, USA, 2000.
[41] P.V. Konarev, V.V. Volkov, A.V. Sokolova, M.H.J. Koch, D.I. Svergun, PRIMUS: A Windows PC-based system for small-angle scattering data analysis, J. Appl. Cryst. 36 (2003) 1277–1282.
[42] DIFFRAC Plus Evaluation package EVA; Version 11; User's Manual; Bruker AXS: Karlsruhe, Germany, 2005.
[43] K.A. Curtis, D. Miller, P. Millard, S. Basu, F. Horkay, P.L. Chandran, Unusual Salt and pH Induced Changes in Polyethylenimine Solutions, PLoS ONE 11 (2016) e0158147.
[44] R.V. Benjaminsen, M.A. Mattebjerg, J.R. Henriksen, S.M. Moghimi, T.L. Andresen, The Possible "Proton Sponge " Effect of Polyethylenimine (PEI) Does Not Include Change in Lysosomal pH, Mol. Ther. 21 (2013) 149–157.
[45] S.V. Fedorenko, A.R. Mustafina, A.R. Mukhametshina, M.E. Jilkin, T.A. Mukhametzyanov, A.O. Solovieva, T.N. Pozmogova, L.V. Shestopalova, M.A. Shestopalov, K.V. Kholin, Y.N. Osin, O.G. Sinyashin, Cellular imaging by green luminescence of Tb(III)-doped aminomodified silica nanoparticles, Mater. Sci. Eng., C 76 (2017) 551–558.
[46] S. Taranejoo, R. Chandrasekaran, W. Cheng, K. Hourigan, Bioreducible PEI-functionalized glycol chitosan: a novel gene vector with reduced cytotoxicity and improved transfection efficiency, Carbohydr. Polym. 153 (2016) 160–168.
[47] A. Verma, F. Stellacci, Effect of surface properties on nanoparticle-cell interactions, Small 6 (2010) 12–21.
[48] O. Harush-Frenkel, N. Debotton, S. Benita, Y. Altschuler, Targeting of nanoparticles to the clathrin-mediated endocytic pathway, Biochem. Biophys. Res. Commun. 353 (2007) 26–32.
[49] S. Veeranarayanan, A.C. Poulose, S. Mohamed, A. Aravind, Y. Nagaoka, Y. Yoshida, T. Maekawa, D.S. Kumar, FITC Labeled Silica Nanoparticles as Efficient Cell Tags: Uptake and Photostability Study in Endothelial Cells, J. Fluoresc. 22 (2012) 537–548.
[50] K. Shapero, F. Fenaroli, I. Lynch, D.C. Cottell, A. Salvati, K.A. Dawson, Time and space resolved uptake study of silicananoparticles by human cells, Mol. BioSyst. 7 (2011) 371–378.
[51] L. Kou, J. Sun, Y. Zhai, Z. He, The endocytosis and intracellular fate of nanomedicines: Implication for rational design, Asian J. Pharm. Sci. 8 (2013) 1–10.
[52] J. Zhu, L. Liao, L. Zhu, P. Zhang, K. Guo, J. Kong, C. Ji, B. Liu, Size-dependent cellular uptake efficiency, mechanism, and cytotoxicity of silica nanoparticles toward HeLa cells, Talanta 107 (2013) 408–415.
[53] M. Beck, F. Förster, M. Ecke, J.M. Plitzko, F. Melchior, G. Gerisch, W. Baumeister, O. Medalia, Nuclear pore complex structure and dynamics revealed by cryoelectron tomography, Science 306 (2004) 1387–1390.
[54] C.W. Pouton, K.M. Wagstaff, D.M. Roth, G.W. Moseley, D.A. Jans, Targeted delivery to the nucleus, Adv. Drug Deliv. Rev. 59 (2007) 698–717.